POLITECNICO
MILANO 1863

SCUOLA DI INGEGNERIA INDUSTRIALE
E DELL'INFORMAZIONE

Executive Summary of the Thesis

Numerical Investigation of the Aerodynamic Interference Effects for a Coaxial Rotor Configuration

Laurea Magistrale in Aeronautical Engineering - Ingegneria Aeronautica

Author: Clara Rondeau Gómez

Advisor: Prof. Luigi Vigevano

Academic year: 2022-2023

1. Introduction

In recent years, the aeronautical industry has embraced the eVTOL concept to provide more intelligent and sustainable mobility options, where its main key feature is the incorporation of multi-propellers. One particular challenge arises from the usage of several propellers nearby: understanding the flow interference between rotors. Hence, a numerical aerodynamics investigation of the interference effects of a coaxial rotor configuration in hover conditions is done to better understand this rotor-rotor interaction. The high-fidelity CFD code ROSITA, created by Politecnico di Milano with a particular emphasis on rotor aerodynamics, is used for the numerical analysis. Its main features include the use of multi-block structured grids, the Chimera technique, and RANS equations. To better understand this rotor-rotor interaction, the performance of an isolated rotor is also being analysed and compared with the coaxial case. In the context of this work, which is also intended to broaden the knowledge of CFD and all its implications, two types of simulations, steady and unsteady, are conducted for the isolated case, where the results of these two setups are presented in an attempt to comprehend the reason behind those differences, if they exist.

Previous numerical studies have been conducted on this specific coaxial configuration [3], more precisely the GARTEUR Action Group HC/AG-26, hence, the validity of the different simulation results is going to be checked.

2. Rotor Aerodynamics Framework

ROSITA (ROtorcraft Software ITAly) is a software specialized mainly in the study of rotor's aerodynamics where unsteady phenomenons occur especially on the wake region. To represent the turbulent characteristics of the flow, it employs a combination of RANS equations with the single-equation Spalart-Allmaras turbulence model. It also uses structured multi-block grids to represent the computational domain, that can be fixed or in relative motion. As the domain is composed of more than one mesh, to compute the connectivity between the different grids, the *Chimera technique* is used. This technique is based on the modified Chesshire and Henshaw algorithm [2].

2.1. Chimera Methods

When having complex geometries, it can be hard or almost impossible to create structured grids with smooth properties, hence, to over-

come these limitations, a partitioning of the domain into simpler overlapping structured subdomains can be carried out thanks to the Chimera technique. This computational approach for solving PDEs is also called *Overset Grid Method* [1]. The process involves categorizing the different points into *Valid Points*, where the PDE is discretized; *Fringe Points*, points in the overlapping regions with other grids where its solution is interpolated from the neighbours, the resultant points are called *Donor Points*; and *Hole Points*, points outside the computational domain. Explicit and implicit interpolation methods are employed for communicating between different grids. The explicit method involves interpolating only from valid points, while the implicit method uses fringe points as donors, requiring the solution of an equation system. The process includes identifying solid wall conditions, using an iterative algorithm to find donor and fringe points, and assigning priority indices to different grids based on their overlapping regions.

3. Computational Model

3.1. Problem Geometry & Set Up

The rotor blade used is an available commercial rotor blade (Xoar model PJN), more specifically, a two-blade 13x7 rotor, having 13 inches or 0.33 m in diameter. For the isolated case, a single Right-Handed Rotor (RHR) is used, where the coordinates' origin lies in the centre of the rotor disk, as shown in Figure 1. R refers to the radius of the propeller, being $R = 0.165$ m

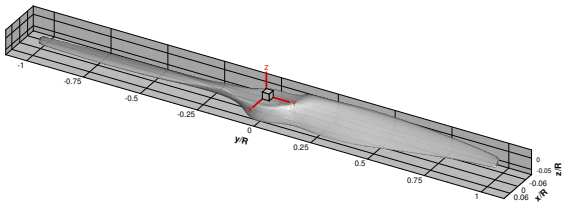

Figure 1: Isolated ISO view

When referring to the coaxial configuration, in this case, a Left-Handed Rotor is used as the upper one, and a Right-Handed for the lower. The lower rotor is placed at $\Delta x = 0$ and $\Delta y = 0$, but with an axial distance from the upper rotor of $\Delta z = -0.5R$, Figure 2. Two different conditions are being tested for both isolated and coaxial configurations, but always keeping the hovering flight condition. A rotating speed of 8'000 rpm and 12'000 rpm. The flow conditions are standardized to the International Standard Atmosphere (ISA) model at mean sea level.

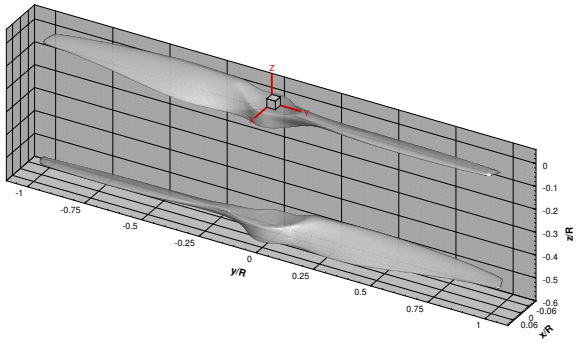

Figure 2: Coaxial ISO view

3.2. Grid Generation and Independence Analysis

The meshing tool used to create the different grids and suitable for the ROSITA CFD solver is the commercial ANSYS ICEM CFD software. To be able to use the Chimera method, three different structured grids have been created. An outer cylindrical grid as the farfield with $r = 12R$ and $L = 24R$, a finer intermediate cylinder to capture the effects of the wake with $r = 2.6D$ and $L = 6D$, and lastly, a mesh surrounding the blade with the proper boundary layer refinement to guarantee a $y^+ \approx 1$. To ensure that the results obtained are not dependent on the different meshes used for the simulation, it is important to perform a mesh independence test. It has only been done for the steady isolated case, as the unsteady simulations require too much computational time. The farfield grid has been kept the same for all configurations, while varying the refinements and number of elements for the mid and blade grids. To know which configuration has the least influence on the results, six different steady simulations for the Isolated case at 8'000 RPM have been done. The error has been computed taking the experimental value from DLR [3] as a reference. After computing all the loads and errors, the configuration with one of the smallest relative errors has been chosen, as it has a good compromise between the fidelity of the results and the total computational cost. Hence, the final grid configuration has 5'418'138 elements for the isolated case, and 7'694'571 elements for the coaxial one.

4. Results & Data Comparison

To better understand the rotor-rotor interaction, unsteady simulations for the two rotors have been computed with different angular velocities. Additionally, data from isolated steady and unsteady simulations have been put in comparison.

4.1. Isolated Rotor

4.1.1 Steady Case

The isolated steady configuration for 8'000 rpm and 12'000 rpm are the first to be computed, as they are the least complex and time-demanding of all the different cases. After 30'000 iterations, the simulations arrive at a stable state, taking 37 hours to converge. Table 1 shows the average values of T and M_z of the different simulations and the experimental values obtained from the DLR AWB group, as shown in Figure 3.

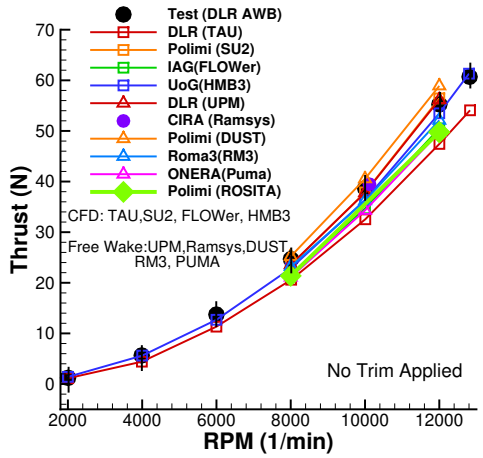

(a) Thrust vs Revolutions

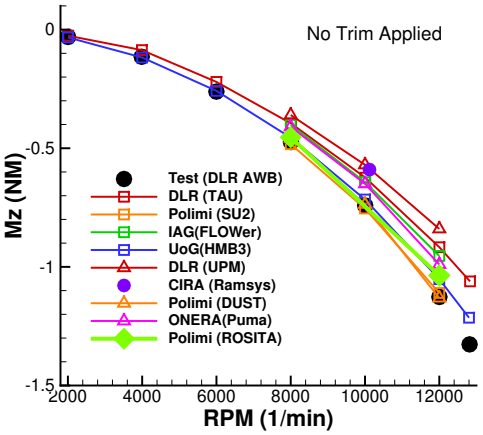

(b) Torque vs Revolutions

Figure 3: Time averaged thrust and torque from [3] along with ROSITA's results.

Evaluating data from Table 1 [3], good results have been obtained with the proposed ROSITA steady code, as they adjust to all computational and experimental data. Hence, some conclusions can be made when studying the flow field for the 12'000 rpm case at the last time step.

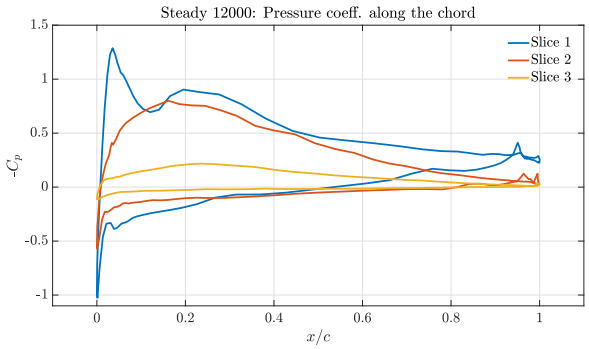

Figure 4: C_p vs x/c for steady 12'000 rpm

Taking the value of the last iteration for the 12'000 rpm case, Figure 4 shows the C_p in three different y locations: one near the tip at $y/R = 0.95$ (Slice 1), one in the middle, $y/R = 0.70$ (Slice 2), and lastly, near the root, $y/R = 0.3$ (Slice 3). The pressure difference between the upper and lower surfaces indicates insignificant loads for the third slice. In the middle position, a standard pressure behaviour is observed with a progressive decrease at the leading edge and recovery towards the trailing edge. High velocities at the rotor blade tip lead to a strong suction peak and intense pressure gradient. However, within this suction region, due to a poor representation of the surface (red circles in Figure 5), the fluid changes its velocity causing pressure variations that lead to a boundary layer separation, creating a recirculating region.

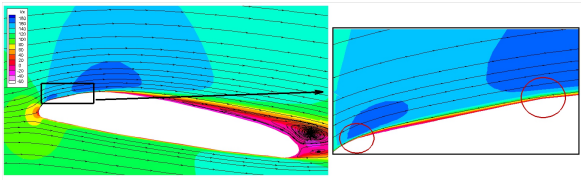

Figure 5: V_x contour at $y/R = 0.95$

To examine the wake region, Figure 6 shows a colour map on the OYZ plane of the vertical velocity and pseudo-stream traces, providing a comprehensive view of the rotor wake. The Froude B.C. can be applied to avoid recirculation in the downstream wake region, which is

not observed. The mean velocity shows the typical contraction of the wake immediately downstream of the rotor disk.

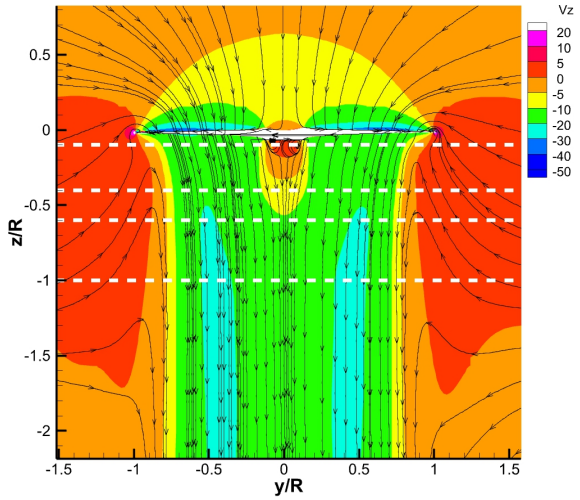

Figure 6: Steady Isolated V_z contour

4.1.2 Unsteady Case

The unsteady simulations have been initialized as a steady state with 500 P-time steps. To achieve a periodical/stable state, 5 revolutions for the are required, with an incremental azimuthal angle of 1 degree and 50 pseudo-time steps for each step. The tagging process has been done once at the beginning, only for one revolution at each azimuthal angle, as it has periodical behaviour. The total computational time was around 88 hours $\approx$ 3.6 days.

Looking at Table 1, if isolated unsteady results are being compared (average values of thrust and torque for the last 2 revolutions), it can be seen that they are in good agreement with the experimental data in [3], and the isolated steady case. After proving the reliability of isolated unsteady simulations for 8'000 rpm and 1'2000 rpm, the flow field from the 12'000 rpm case is analysed using the data from the last time step, the azimuthal angle being $\Phi = 1800^{o}$.

The C_p plot along the chord on different y/R for the unsteady case is not presented, as has the same shape as for the steady case, in other words, the pressure coefficient at the rotor's surface behaves similarly for both setups.

The wake region is being again studied by plotting the OYZ colour map of the vertical velocity along with its pseudo-streamtraces in Figure 7. As the *Froude B.C.* at the far-field is not yet implemented in unsteady simulations, hence the *Farfield B.C.* is used, causing the flow to recirculate inside the domain. The presence of vortices near the rotor disk for the first revolutions causes the wake flow field region to not have steady behaviour. Hence, more revolutions are needed to obtain a stable wake region flow field. The wake contraction has also been captured by looking at the inward deflection of the pseudo streamtraces.

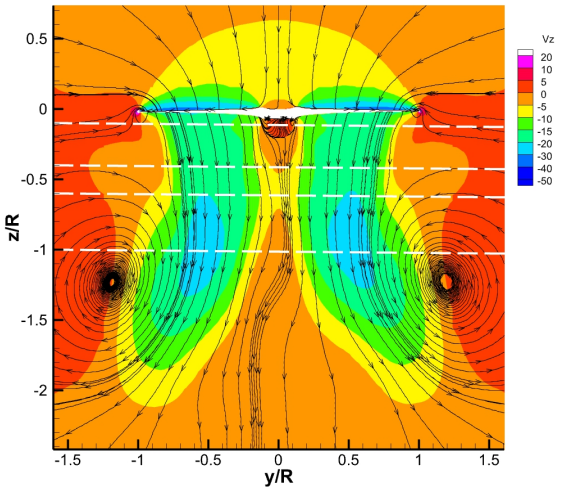

Figure 7: Unsteady Isolated V_z contour

Figure 8 shows the vertical velocity trend at the OYZ plane in two different z for the unsteady case against the steady case. The first z-plane, right after the rotor disk, shows the same behaviour as the steady case, but the wake region dissipation becomes stronger when moving downstream due to the presence of the recirculation wake vortices. This trend intensifies at $z = -1R$, where the steady wake shear layer is still well-defined, however, for the unsteady case, the wake region is being dissipated by moving the fluid outwards and decelerating in the central part. Again, more revolutions for the unsteady case are needed to obtain a similar shear layer wake region as the steady case.

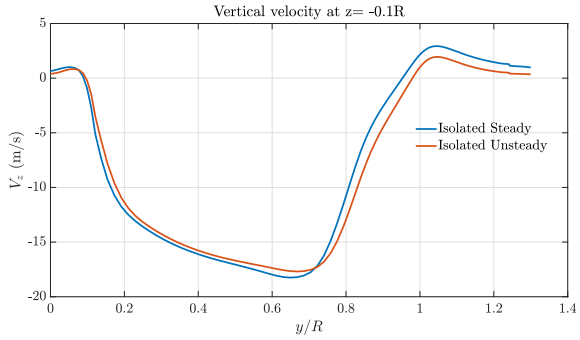

(a) Vertical velocity at z = -0.1R

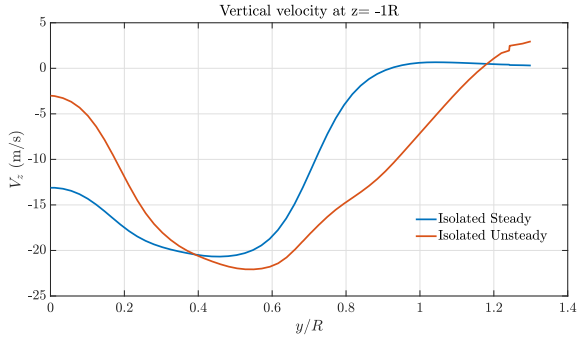

(b) Vertical velocity at z = -1R

Figure 8: Steady vs Unsteady V_z at different z

4.2. Coaxial Rotor

Once the performance of the isolated rotor has been analysed, it is time to add a second rotor to evaluate the performance of the coaxial configuration. A total of 7 revolutions has been computed for both cases. The total computational time has been around 135 hours = 5.6 days.

Looking at Table 1, some conclusions can be made: for the coaxial configuration, one can detect a loss of thrust on the lower rotor compared with the upper one. This behaviour primarily results from the impact of the downwash from the upper rotor, where the upper-induced velocity causes a reduction of the effective angles of attack of the lower rotor. Additionally, there is a slight reduction of the upper rotor thrust because of the mutual interaction with the lower rotor.

Figure 9 shows an oscillating behaviour throughout a revolution, this is due to the mutual aerodynamic interference between the upper and lower rotor, associated with the periodical passage of the blades over each other (4 times per revolution: 0º, 90º, 180º and 270º), resulting in a pulsation in the aerodynamic loads.

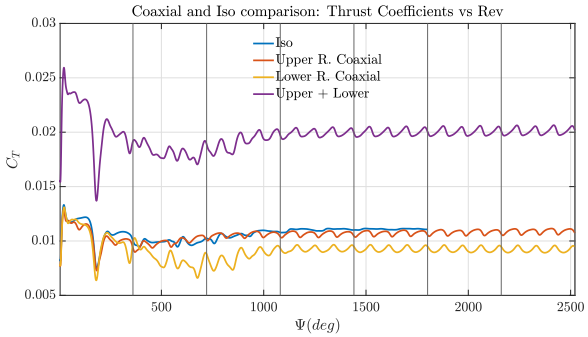

Figure 9: C_T evolution through Φ

Figure 9 shows an oscillating behaviour throughout a revolution, this is due to the mutual aerodynamic interference between the upper and lower rotor, associated with the periodical passage of the blades over each other (4 times per revolution: 0º, 90º, 180º and 270º), resulting in a pulsation in the aerodynamic loads.

To better understand the rotor-rotor interference of two contra-rotating rotors, and how the dynamics of each rotor modify the flowfield, the C_p at different y/R surfaces has been plotted in Figure 10.

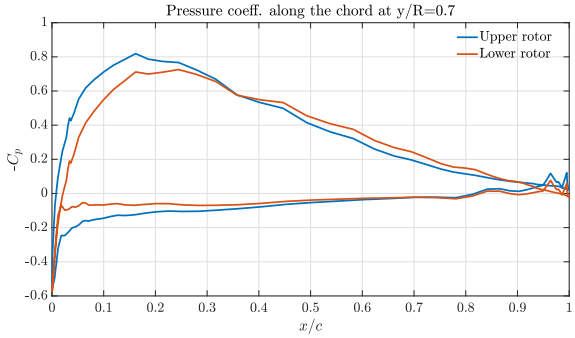

(a) C_p vs x/c at $y/R = 0.7$

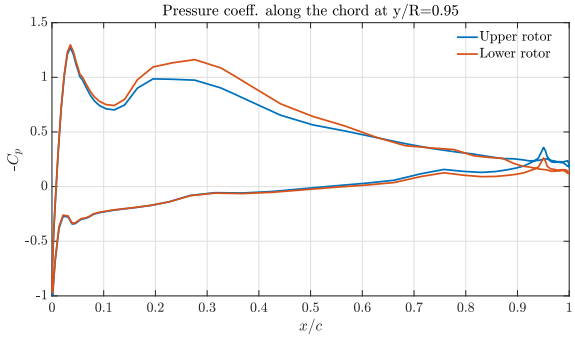

(b) C_p vs x/c at $y/R = 0.95$

Figure 10: Coaxial C_p behaviour at $\Phi = 2520º$

Due to the induced velocity of the upper rotor, the lower one suffers a reduction of the effective angle of attack and, consequently, a reduction

of the total thrust. This behaviour is mostly reflected in Figure 10a, where the difference of pressure between the upper and lower surface from the lower rotor has decreased with respect to the upper one. Also, as the effective angle has also been reduced, there is a more progressive decrease in pressure and a less intense suction peak. At 95% of the rotor-blade span, in both cases, there is a strong suction peak and a non-gradual pressure recovery where the fluid accelerates and slows down, as seen for the isolated cases. Despite the poor representation of the surface, a higher acceleration of the fluid is perceived in the lower rotor. This faster inflow velocity is due to the ingestion of the upper rotor wake that produces an acceleration of the flow.

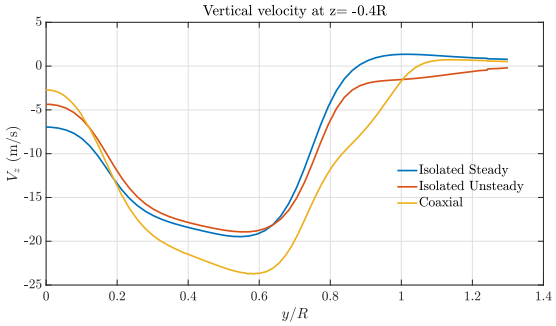

(a) V_z at z = -0.4R

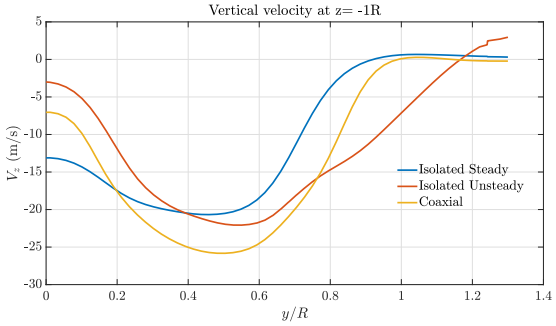

(b) V_z at z = -1R

Figure 11: Isolated vs coaxial V_z at different z at $\Phi = 2520^{o}$

Figure 11, shows the vertical velocity plot at the OYZ plane. Right after the upper rotor disk, the coaxial configuration shows similar characteristics of the flow field compared to the isolated cases, as little influence of the lower rotor is perceived. When approaching the lower rotor, $z = -0.4R$, there is an acceleration of the flow due to the relative motion of the rotor, which creates a suction zone in the upper surface. Once the flow has passed through the second rotor, new dynamic variations in the shear layer occur, which are produced by the additional induced velocity of this second rotor. However, far from the rotors, $z = -1R$, the contraction of the wake along with higher velocities is still present for the coaxial case, whereas, the velocity dissipation for the unsteady isolated is more pronounced.

	rpm	DLR Test	Steady Isolated	Unsteady Isolated	Coaxial Upper rotor	Coaxial Lower rotor
T (N)	**8000**	24.677	21.147	21.369	20.88	17.63
	12000	55.250	49.352	49.759	48.16	41.19
Mz (Nm)	**8000**	-0.474	-0.450	-0.453	-0.455	-0.563
	12000	-1.127	-1.052	-1.036	-1.047	-1.069

Table 1: Average values for all cases studied

5. Conclusions

The aim of this research is the study of the flow interaction between coaxial rotors in hover conditions, and apply this knowledge within the eVTOL sector. The in-house ROSITA CFD software has been used to predict the flow field, based on RANS equations and multi-block structured grids. To gain a deeper understanding of flow dynamics in a coaxial configuration, it has been crucial to examine the isolated rotor and compare its performance with the coaxial one.

Results from steady and unsteady isolated simulations have been compared, finding that for a single rotor, the steady setup is a better choice due to its less complex and time-consuming nature, and obtaining a slightly better prediction of the wake flowfield. To have a better representation of the wake for the unsteady case, more revolutions need to be computed until reaching a periodical behaviour of the loads, and avoiding detached vortices caused by the initial unsteady motion of the fluid.

Plotting different parameters such as pressure coefficient, velocity contour, and pseudo-streamtraces have revealed a poor discretization of the tip's surface, causing the fluid in that region to compress and expand followed by a boundary layer separation. A smoother surface would have caused a more gradual pressure recovery and less intense boundary layer separation.

As there are two counter-rotating rotors, the simulation must be unsteady, making the total computational cost quite expensive due to the high total number of elements and the periodi-

cal tagging process. The rotor-rotor interaction has been captured as a pulsation in the aerodynamic loads plot through the revolutions. Moreover, a loss of thrust on the lower rotor compared with the upper one has been observed. This behaviour primarily results from the impact of the downwash, where the upper rotor-induced velocity causes a reduction of the effective angles of attack of the lower rotor.
A solid match of ROSITA's results with data from [3] has confirmed the reliability of the code when simulating the aerodynamics of isolated and coaxial rotors. In conclusion, satisfactory results have been achieved by accurately capturing the rotor-rotor interaction, making this investigation primarily serve as a base for future works.

References

[1] William Chan, Reynaldo Gomez, Stuart Rogers, and Pieter Buning. Best practices in overset grid generation. In *32nd AIAA Fluid Dynamics Conference and Exhibit*, page 3191, 2002.

[2] G Chesshire and W.D Henshaw. Composite overlapping meshes for the solution of partial differential equations. *Journal of Computational Physics*, 90(1):1–64, 1990.

[3] Jianping Yin, F. De Gregorio, Karl-Stephane Rossignol, Lukas Rottmann, Giuseppe. Ceglia, Gabriel Reboul, G. Barakos, G. Qiao, M. Muth, M. Kessler, A. Visingardi, M. Barbarino, F. Petrosino, Alex Zanotti, N. Oberti, L. Galimberti, Giovanni Bernardini, Caterina Poggi, L. Abergo, F. Caccia, A. Guardone, Claudio Testa, and S. Zaghi. Acoustic and aerodynamic evaluation of dlr small-scale rotor configurations within garteur ag26. In *49th European Rotorcraft Forum, ERF 2023*, September 2023.